Article

Photodissociation Dynamics of Fluorobenzene

Cheng-Liang Huang, Jyh-Chiang Jiang, Alexander M. Mebel, Yuan T. Lee, and Chi-Kung Ni

J. Am. Chem. Soc., **2003**, 125 (32), 9814-9820• DOI: 10.1021/ja030185k • Publication Date (Web): 19 July 2003

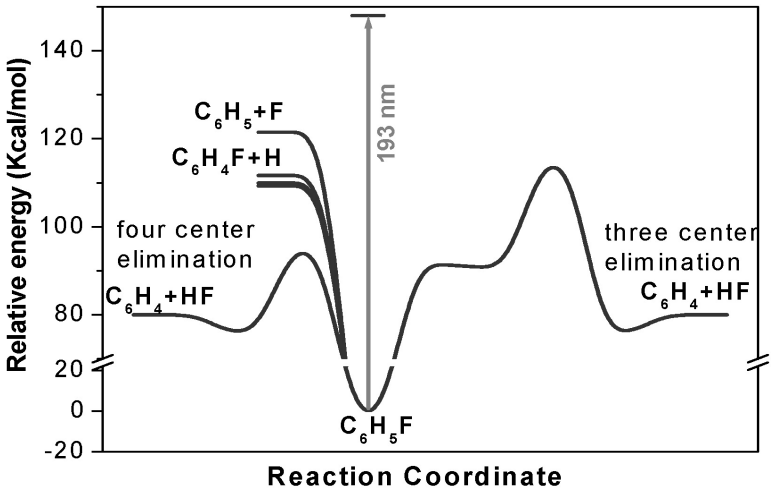

More About This Article

Additional resources and features associated with this article are available within the HTML version:

- Supporting Information
- Links to the 4 articles that cite this article, as of the time of this article download
- Access to high resolution figures
- Links to articles and content related to this article
- Copyright permission to reproduce figures and/or text from this article

View the Full Text HTML

J|A|C|S
ARTICLES
Published on Web 07/19/2003

Photodissociation Dynamics of Fluorobenzene

Cheng-Liang Huang,[†] Jyh-Chiang Jiang,[‡] Alexander M. Mebel,[†] Yuan T. Lee,[†,§] and Chi-Kung Ni*,[†]

Contribution from the Institute of Atomic and Molecular Sciences, Academia Sinica, P.O. Box 23-166, Taipei, Taiwan, ROC, National Taiwan University of Science and Technology, Taipei 106, Taiwan, ROC, and Chemistry Department, National Taiwan University, Taipei, Taiwan, ROC

Received March 21, 2003; E-mail: ckni@po.iams.sinica.edu.tw

Abstract: Photodissociation of both fluorobenzene and d_5-fluorobenzene at 193 nm under collision-free conditions has been studied in separate experiments using multimass ion imaging techniques. HF and DF eliminations were found to be the major dissociation channels. Small amounts of photofragments, C_6H_4F and C_6D_4F, corresponding to H and D atom eliminations were also observed. Dissociation rate and fragment translational energy distribution suggest that HF (DF) and H (D) atom elimination reactions occur in the ground electronic state. The potential energy surface obtained from ab initio calculations indicates that the four-center reaction in the ground electronic state is the major dissociation mechanism for the HF and DF eliminations. A comparison with photodissociation of benzene has been made.

I. Introduction

Today, aromatic photochemistry is a major area of study. The conspicuous feature that has emerged from the studies of aromatic photochemistry is that the photoexcitation of the benzene ring leads to a rich variety of reactions. Photoexcitation of benzene at 193 nm correlates to the excitation of a phenyl ring. H atom and H_2 molecule eliminations are the two unimolecular dissociation channels that are energetically possible to occur.[1] However, only H atom elimination was observed.[2] At higher excitation energy, extensive isomerization followed by complicated dissociation channels, such as $C_6H_6 \rightarrow C_4H_3 + C_2H_3$, $C_6H_6 \rightarrow C_5H_3 + CH_3$, $C_6H_6 \rightarrow 2C_3H_3$, and $C_6H_6 \rightarrow C_4H_4 + C_2H_2$, have been observed in molecular beam experiments.[2,3] Photodissociation of d_3-toluene at 193 nm is another example that demonstrates the complexity of dissociation reactions in aromatic molecules. In addition to the fragments produced from the major channels, $C_6H_5CD_3 \rightarrow C_6H_5CD_2 + D$ and $C_6H_5CD_3 \rightarrow C_6H_5 + CD_3$,[4−10] the CD_2H, CDH_2, CH_3, $C_6D_3H_2$, $C_6D_2H_3$, C_6DH_4, and $C_7H_4D_3$ fragments were also observed.[11] This shows that about 25% of the excited toluene isomerizes to a seven-membered ring (cycloheptatriene) and then rearomatizes prior to dissociation. This newly observed isomerization is totally different from all the other isomerization mechanisms of aromatic molecules.[12−17] The significance of this isomerization is that during isomerization the carbon atoms and hydrogen atoms belonging to the alkyl group are involved in an exchange with those atoms in the aromatic ring. The similar isomerization−dissociation mechanism has also been observed in xylene.[18] For molecules with larger alkyl groups such as ethylbenzene, propylbenzene, and ethyltoluene, the C−C bond in the alkyl group is the weakest chemical bond and the dissociation occurs mainly through the cleavage of the C−C bond.[19−26] However, the dissociation mechanism of the S_1 state is different from that of the S_2 state.[27,28] Molecules excited to the S_2 state were found to be completely dissociated in the ground state

[†] Academia Sinica.
[‡] National Taiwan University of Science and Technology.
[§] National Taiwan University.

(1) Mebel, A. M.; Lin, M. C.; Chakraborty, D.; Park, J.; Lin, S. H.; Lee, Y. T. *J. Chem. Phys.* **2001**, *114*, 8421−8435.
(2) Tsai, S. T.; Huang, C. L.; Lee, Y. T.; Ni, C. K. *J. Chem. Phys.* **2001**, *115*, 2449−2455.
(3) Hsu, T. C.; Shu, J. N.; Chen, Y.; Lin, J. J.; Lee, Y. T.; Yang, X. M. *J. Chem. Phys.* **2001**, *115*, 9623−9636.
(4) Hippler, H.; Schubert, V.; Troe, J.; Wendelken, H. *J. Chem. Phys. Lett.* **1981**, *84*, 253−256.
(5) Park, J.; Bersohn, R.; Oref, I. *J. Chem. Phys.* **1990**, *93*, 5700−5708.
(6) Fröchtenicht, R. *J. Chem. Phys.* **1994**, *102*, 4850−4859.
(7) Nakashima, N.; Yoshihara, K. *J. Phys. Chem.* **1989**, *93*, 7763−7771.
(8) Luther, K.; Troe, J.; Weitzel, K. L. *J. Phys. Chem.* **1990**, *94*, 6316−6320.
(9) Brand, U.; Hippler, H.; Lindemann, L.; Troe, J. *J. Phys. Chem.* **1990**, *94*, 6305−6316.
(10) Shimada, T.; Ojima, Y.; Nakashima, N.; Izawa, Y.; Yamanaka, C. *J. Phys. Chem.* **1992**, *96*, 6298−6302.
(11) Lin, C. K.; Huang, C. L.; Jiang, J. C.; Chang, A. H. H.; Lee, Y. T.; Lin, S. H.; Ni, C. K. *J. Am. Chem. Soc.* **2002**, *124*, 4068−4075.
(12) Wilzbach, K. E.; Kaplan, L. *J. Am. Chem. Soc.* **1964**, *86*, 2307−2308.
(13) Burgstahler, A. W.; Chien, P. L. *J. Am. Chem. Soc.* **1964**, *86*, 2940−2941.
(14) Kaplan, L.; Wilzbach, K. E.; Brown, W. G.; Yang, S. S. *J. Am. Chem. Soc.* **1965**, *87*, 675−676.
(15) Wilzbach, K. E.; Kaplan, L. *J. Am. Chem. Soc.* **1965**, *87*, 4004−4006.
(16) Den Besten, I. E.; Kaplan, L.; Wilzbach, K. E. *J. Am. Chem. Soc.* **1968**, *90*, 5868−5872.
(17) Bryce-Smith, D.; Gilbert, A. In *Rearrangement in Ground and Excited States*, Vol. 3; De Mayo, P., Ed.; Academic Press: New York, 1980.
(18) Huang, C. L.; Jiang, J. C.; Lee, Y. T.; Ni, C. K. *J. Phys. Chem. A* **2003**, *107*, 4019−4024.
(19) Kajii, Y. K.; Tanaka, Obi, I.; Ikeda, N.; Nakashima, N.; Yoshihara, K. *J. Chem. Phys.* **1987**, *86*, 6115−6118.
(20) Nakashima, N.; Yoshihara, K. *J. Phys. Chem.* **1989**, *93*, 7763−7771.
(21) Tsukiyama, K.; Bersohn, R. *J. Chem. Phys.* **1987**, *86*, 745−749.
(22) Park, J.; Bersohn, R.; Oref, I. *J. Chem. Phys.* **1990**, *93*, 5700−5708.
(23) Br, U.; Hippler, H.; Lindemann, L.; Troe, J. *J. Phys. Chem.* **1990**, *94*, 6305−6316.
(24) Luther, K.; Troe, J.; Weitzel, K. L. *J. Phys. Chem.* **1990**, *94*, 6316−6320.
(25) Lange, S.; Luther, K.; Rech T.; Schmoltner, A. M.; Troe, J. *J. Phys. Chem.* **1994**, *98*, 6509−6513.
(26) Shimada, T.; Ojima, Y.; Nakashima, N.; Izawa, Y.; Yamanaka, C. *J. Phys. Chem.* **1992**, *96*, 6298−6302.
(27) Huang, C. L.; Jiang, J. C.; Lin, S. H.; Lee, Y. T.; Ni, C. K. *J. Chem. Phys.* **2002**, *116*, 7779−7782.

10.1021/ja030185k CCC: $25.00

after internal conversion, while most of the molecules (70%−80%) excited to the S_1 state dissociate in the triplet state through intersystem crossing and the rest of the molecules dissociate in the ground state.

In contrast to benzene and toluene, the photodissociation of phenyl halides shows the simple dissociation products. Ultraviolet (UV) absorption of the phenyl halides (−Cl, −Br, −I) in the 190 nm−250 nm range corresponds to the excitations of electrons of the phenyl ring and the nonbonding electron of the halogen atoms. The nonbonding electron excitation of the halogen atoms leads to direct dissociation, that is, an immediate release of halogen atoms on a repulsive surface. Alternately, the excitation of the phenyl ring results in an excited state, stable with respect to dissociation. Dissociation occurs indirectly either through the coupling of the stable and repulsive state or after the internal conversion from an initial excited state to a lower electronic state. Direct dissociation is fast and releases a large amount of kinetic energy. Indirect dissociation results in a limited release of kinetic energy due to the extensive energy randomization among vibrational degrees of freedom and has a slow dissociation rate. Statistical transition-state theory has predicted that, given comparable pre-exponential factors for different bond fissions, the reaction pathway with the lowest energetic barrier should dominate the indirect dissociation. Since the C−X (X = Cl, Br, I) bond energy is relatively small, halogen atom elimination is expected to be the major channel in the indirect dissociation. In the photodissociation of iodobenzene,[29,30] bromobenzene,[30,31] chlorobenzene,[30,32−35] *o*-, *m*-, *p*-chlorotoluene,[35−38] and *o*-, *m*-, *p*-dichlorobenzene,[37,39,40] halogen atom elimination indeed was found to be the only dissociation channel, and both direct and indirect dissociation have been observed.

Compared to the other phenyl halides, the photochemistry of fluorine atom substituted benzenes has received little attention. Since the fluorine atom is not an electronic chromophore in 190 nm−250 nm, the UV absorption only correlates to the excitation of the phenyl ring. Therefore, an immediate release of F atom on a repulsive surface does not occur. In addition, the C−F bond has a very high dissociation threshold and F atom elimination from the ground state after internal conversion is not expected to occur. As a result, the dissociation mechanism in this photon energy region should be very different from those of the other phenyl halides. On the other hand, one would expect that the photodissociation mechanism of fluorobenzene could be similar to that of benzene, since both of them correlate to the excitation of the phenyl ring and the weakest chemical bond in both molecules is the C−H bond. In this paper, multimass ion imaging techniques have been employed to investigate the photodissociation of fluorobenzene at 193 nm in a molecular beam. The results demonstrate that the dissociation of fluorobenzene is not only different from those of the other phenyl halides but also very different from that of benzene.

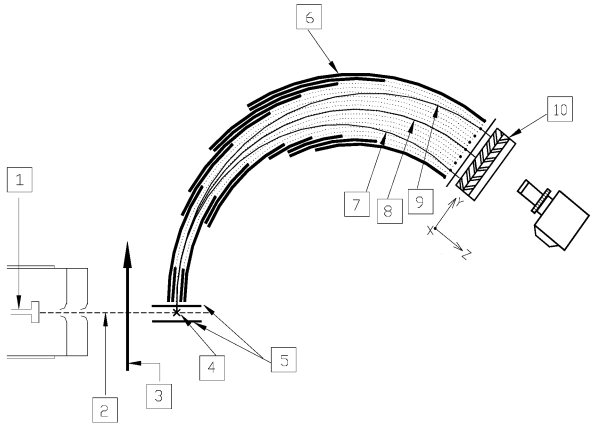

Figure 1. Schematic diagram of the multimass ion imaging detection system. (1) nozzle; (2) molecular beam; (3) photolysis laser beam; (4) VUV laser beam, which is perpendicular to the plane of the paper; (5) ion extraction plates; (6) energy analyzer; (7−9) simulation ion trajectories of $m/e = 16$, 14, and 12; (10) Two-dimensional detector, where *Y*-axis is mass axis and *X*-axis (perpendicular to the plane of the paper) is the velocity axis.

II. Experiment

The experimental techniques have been described in detail in our previous reports on other aromatic molecules,[28,41,42] and only a brief description is given here. Fluorobenzene vapor was formed by flowing ultrapure Ar at pressures of 300 Torr through a reservoir filled with liquid sample at 10 °C. The fluorobenzene/Ar mixture was then expanded through a 500 μm high-temperature (90 °C) pulsed nozzle to form the molecular beam. Molecules in the molecular beam were photodissociated by an UV laser pulse. Due to the recoil velocity and center-of-mass velocity, the fragments were expanded to a larger sphere on their flight to the VUV laser beam and then ionized by a VUV laser pulse. The distance and time delay between the VUV laser pulse and the photolysis laser pulse were set such that the VUV laser beam passed through the center-of-mass of the dissociation products and generated a line segment of photofragment ions through the center-of-mass of the dissociation products by photoionization. The length of the segment was proportional to the fragment recoil velocity in the center-of-mass frame multiplied by the delay time between the photolysis and the ionization laser pulses. To separate the different masses within the ion segment, a pulsed electric field was used to extract the ions into a mass spectrometer after ionization. While the mass analysis was being executed in the mass spectrometer, the length of each fragment ion segment continued to expand in the original direction according to its recoil velocity. At the exit port of the mass spectrometer, a two-dimensional ion detector was used to detect the ion positions and intensity distribution. In this two-dimensional detector, one direction was the recoil velocity axis and the other was the mass axis. The schematic diagram of the experimental set up is shown in Figure 1.

According to the velocity of the molecular beam, it was necessary to change the distance between the photolysis laser beam and the VUV

(28) Huang, C. L.; Jiang, J. C.; Lee, Y. T.; Ni, C. K. *J. Chem. Phys.* **2002**, *117*, 7034−7040.
(29) Dzvonik, M.; Yang, S.; Bersohn, R. *J. Chem. Phys.* **1974**, *61*, 4408−4421.
(30) Freedom, A.; Yang, S. C.; Kawasaki, M.; Bersohn, R. *J. Chem. Phys.* **1980**, *72*, 1028−1033.
(31) Zhang, H.; Zhu, R. S.; Wang, G. J.; Han, K. L.; He, G. Z.; Lou, N. Q. *J. Chem. Phys.* **1999**, *110*, 2922−2927.
(32) Han, K. L.; He, G. Z.; Lou, N. Q. *Chem. Phys. Lett.* **1993**, *203*, 509−514.
(33) Wang, G. J.; Zhu, R. S.; Zhang, H.; Han, K. L.; He, G. Z.; Lou, N. Q. *Chem. Phys. Lett.* **1998**, *288*, 429−432.
(34) Ichimura, T.; Mori, Y.; Shinohara, H.; Nishi, N. *Chem. Phys.* **1994**, *189*, 117−125.
(35) Ichimura, T.; Mori, Y.; Shinohara, H.; Nishi, N. *Chem. Phys. Lett.* **1985**, *122*, 51−54.
(36) Kawasaki, M.; Kasatani, K.; Sato, H.; Shinohara, H.; Nishi, N. *Chem. Phys.* **1984**, *88*, 135−142.
(37) Ichimura, T.; Mori, Y.; Shinohara, H.; Nishi, N. *J. Chem. Phys.* **1997**, *107*, 835−842.
(38) Satyapal, S.; Tasaki, S.; Bersohn, R. *Chem. Phys. Lett.* **1993**, *203*, 349−352.
(39) Zhu, R. S.; Zhang, H.; Wang, G. J.; Gu, X.; Han, K. L.; He, G. Z.; Lou, N. Q. *Chem. Phys.* **1999**, *248*, 285−292.
(40) Ichimura, T.; Shimoda, A.; Kikuchi, T.; Kohso, Y.; Hikid, T.; Mori, Y. *J. Photochem.* **1985**, *31*, 157.
(41) Tsai, S. T.; Lin, C. K.; Lee, Y. T.; Ni, C. K. *Rev. Sci. Instrum.* **2001**, *72*, 1963−1969.
(42) Tsai, S. T.; Lee, Y. T.; Ni, C. K. *J. Phys. Chem. A.* **2000**, *104*, 10125−10130.

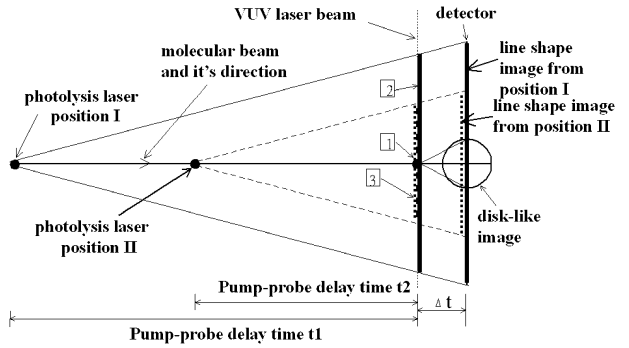

Figure 2. Relationship between the lengths of the image that resulted from different crossing points of the photolysis laser with the molecular beam. The disklike image from the dissociation after ionization was also shown. (1) The crossing point of the molecular beam and the VUV laser beam, where the dissociative ionization (reaction 6∼8) occurs. The disklike image is from these dissociative ionizations. (2 and 3) The lengths of fragment ion distribution created by the VUV laser photoionization from photolysis laser at position I and position II, respectively. The line shape images are from these fragment ion distribution. The variables t_1 and t_2 represent two different delay times between the photolysis laser pulse and the VUV laser pulse according to two different photolysis laser positions. Δt is the flight time of fragment ion in the mass spectrometer.

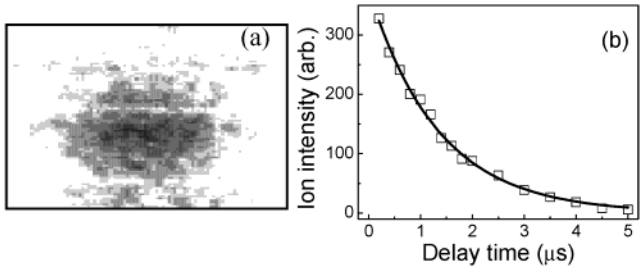

Figure 3. (a) Images of $m/e = 70$ ($C_4H_3F^+$). (b) Intensity decay of the image as a function of delay time.

laser beam to match the delay time between these two laser pulses to ensure that the ionization laser would pass through the center-of-mass of the products. The change of the distance between the two laser beams changed the length of the fragment ion segment in the image. The relationship between the length of the ion image and the position of the photolysis laser is illustrated in Figure 2. If the molecules were not dissociated after the absorption of UV photons, these high internal energy molecules would remain within the molecular beam. They flew with the same velocity (molecular beam velocity) to the ionization region and were ionized by the VUV laser. The wavelength of the VUV laser in this experiment was set at 118.2 nm such that the photon energy was only large enough to ionize parent molecules. The dissociation of parent molecule cations would not occur with the energy left after the VUV laser ionization. However, the dissociation occurred following the 118.2 nm VUV laser ionization for those hot molecules, which absorbed UV photons without dissociation. The ion image of the dissociative ionization was different from the image due to the dissociation products of neutral parent molecules. Since ionization and dissociation occurred at the same position, the image of dissociative ionization was a 2D projection of the photofragment ion's 3D-recoil velocity distribution. It was very similar to the image from the conventional ion imaging techniques and was a disklike image, rather than a line-shape image. In addition, the size of image from the dissociative ionization would not change with the delay time. From the shape of the image and its change with the delay time, the image from dissociation of neutral molecules can easily be distinguished from the dissociative ionization image.

The dissociation rate can be obtained from the product growth with respect to the delay time between the pump and probe lasers using a time-of-flight mass spectrometer. However, accurate measurement can

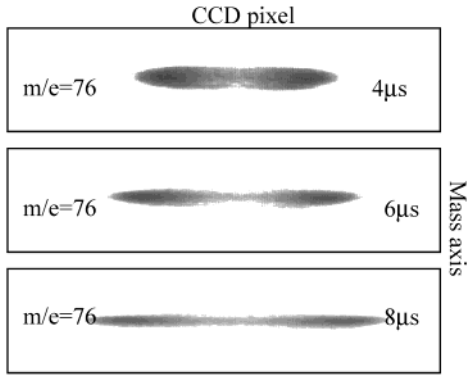

Figure 4. Images of $m/e = 76$ ($C_6H_4^+$) at various delay times.

be obtained only when the dissociation rate is fast enough before the parent molecules and fragments fly out of the detection region due to the molecular beam velocity and recoil velocity, respectively. Another approach is to measure the disappearance rate of the parent molecules, that is, the intensity change of the disklike images at various delay times along the molecular beam.[44] In this work, both of these methods were used to obtain the rate constants.

III. Computational Method

All ab initio calculations were processed with the GAUSSIAN 98 program. The geometry optimization and vibrational frequencies of the reactants, transition states, intermediates, and products were calculated by using the Becke3LYP level with 6-31+G*. The minima (number of imaginary frequencies NIMAG = 0) and first-order saddle points (number of imaginary frequencies NIMAG = 1) were confirmed through the calculations of harmonic vibrational frequencies, which were also used to obtain zero-point vibrational energies. To establish more reliable energy results, single-point calculations were performed at the B3LYP/aug-cc-pVTZ level using the B3LYP/6-31+G* equilibrium geometries.

IV. Results

A. C_6H_5F. Fragment ions of m/e =70, 76, and 95 were observed from the photodissociation of C_6H_5F at 193 nm. Figure 3(a) shows the image of mass $m/e = 70$ ($C_4H_3F^+$). The shape of the image is disklike; therefore, it must result from the dissociation of excited fluorobenzene after ionization. This cation dissociation channel has been observed in previous studies.[43,44] The dissociation rate of the neutral excited fluorobenzene molecules due to the 193 nm photon excitation was measured from the intensity change of these disklike images at various delay times. A dissociation rate of $(8 \pm 3) \times 10^5$ s^{-1}, corresponding to the lifetime 1.2 μs, was obtained, as shown in Figure 3b.

Fragment ion $m/e = 76$ ($C_6H_4^+$) has the largest ion intensity. The images at various delay times are shown in Figure 4. As the delay time between pump and probe laser pulses increased, the length of the image increased rapidly. This is the C_6H_4 fragment that resulted from the dissociation of neutral excited fluorobenzene, corresponding to the HF elimination. A dissociation rate of $(1.4 \pm 0.8) \times 10^6$ s^{-1} was obtained from the product growth with respect to the delay time between pump and probe laser pulses, as shown in Figure 5. The uncertainty of the rate measurement is largely due to the fast escape of product from the detection region. However, the similar

(43) Howe, I.; Williams, D. H. *J. Am. Chem. Soc.* **1969**, *91*, 7137.
(44) Nishimura, T.; Meisels, G.; Niwa, Y. *Bull. Chem. Soc. Jpn.* **1991**, *64*, 2894.

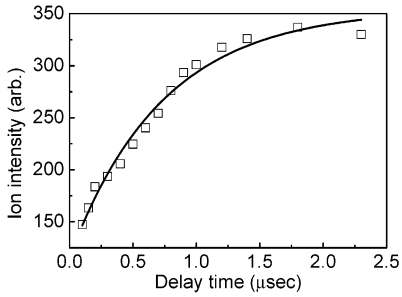

Figure 5. Product C_6H_4 growth with respect to the delay time between pump and probe pulses.

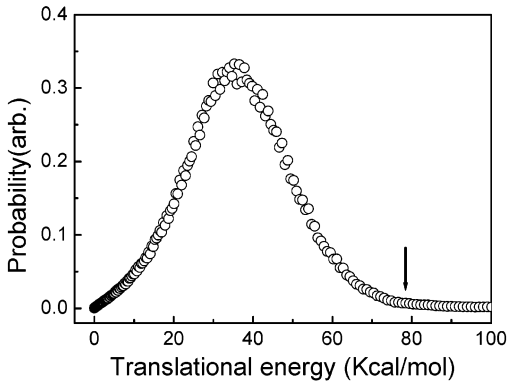

Figure 6. Photofragment translational energy distribution of the reaction $C_6H_5F + h\nu_{193nm} \rightarrow C_6H_4 + HF$. The arrow indicates the maximum available energy.

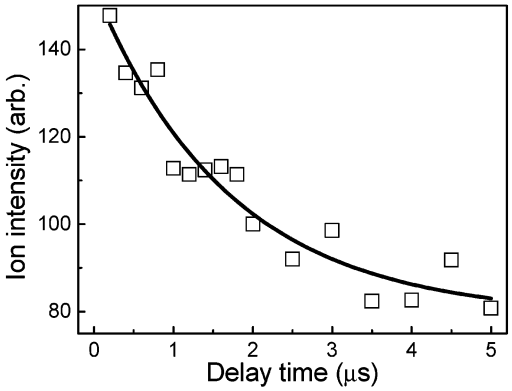

Figure 7. Fragment ion intensity decay of $m/e = 95$.

dissociation rates of $m/e = 70$ and 76 indicate that they must be from the same electronic state.

The photofragment translational energy distribution of the HF elimination is shown in Figure 6. The average released translational energy is large, and the peak of the distribution is located at 37 kcal/mol. The maximum translational energy reaches the maximum available energy of the reaction $C_6H_5F \rightarrow C_6H_4 + HF$. Since the fragment maximum translational energy corresponds to the products C_6H_4 and HF produced in the ground electronic state and the ground state of these two close shell fragments only correlates to the ground state of the parent molecule, the dissociation must result from the ground electronic state.

The fragment ion intensity decay of $m/e = 95$, corresponding to a dissociation rate of $(7 \pm 2) \times 10^5$ s^{-1}, was obtained, as shown in Figure 7. The value of the rate indicates that it comes in the same electronic state as that of the HF elimination channel. The non-zero intensity of $m/e = 95$ ($C_6H_4F^+$) at a long delay

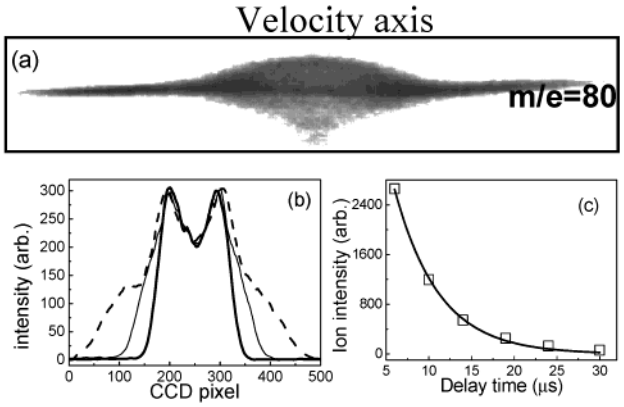

Figure 8. (a) Image and (b) image intensity profiles of fragment ion $m/e = 80$ ($C_6D_4^+$) at various delay times. Thick solid line, thin solid line, and dashed line represent the delay time of 6, 12, and 20 μs, respectively. The ion intensities have been normalized. (c) Image intensity decay of the central component $m/e = 80$.

time suggests the existence of the H atom elimination channel of neutral excited fluorobenzene. Unfortunately, the image of $m/e = 95$ showed strong interference by the parent ion due to the small $m/e = 95$ signal and large parent ion intensity, as well as the limited mass resolution. Other evidence for supporting the H atom elimination can be seen from the d_5-fluorobenzene in the next paragraph.

The fragment ion intensity of C_6H_4 is 25 times larger than that of C_6H_4F. This value has been corrected for the fragment velocity effect. The branching ratios can be obtained directly from the normalization of these values by the ionization cross sections at this wavelength. Although we do not have the ionization cross sections for these fragments at this moment, the large difference of the ion intensities between these two fragments indicates HF elimination is the major channel.

B. C_6D_5F. The similar dissociation channels were also observed in the photodissociation of C_6D_5F with a small difference in dissociation rates. The shape of the image $m/e = 73$ ($C_4D_3F^+$) was disklike, and the dissociation rate obtained from the intensity decay of these disklike images is $(1.8 \pm 0.5) \times 10^5$ s^{-1}. Note that this decay rate is 4 times slower than that of C_6H_5F.

The image and the image intensity profiles of fragment ion $m/e = 80$ ($C_6D_4^+$) at various delay times are shown in Figure 8a and b, respectively. They show little difference from those for $C_6H_4^+$. It is clear that the fragment image has two components. A line shape image superimposed on the disklike image was observed. As the delay time between pump and probe laser pulses increased, the line shape component on both wings moved rapidly toward the outside. They are the fragments resulted from dissociation of neutral fluorobenzene. However, the size of the disklike component located at the center did not change. This disklike component resulted from the dissociative ionization of undissociated excited fluorobenzene by VUV photoionization. The decay rate of this center component, as shown in Figure 8c, was found to be $(1.9 \pm 0.6) \times 10^5$ s^{-1}. The photofragment translational energy distribution of the component on both wings is shown in Figure 9. The distribution below 17 kcal/mol cannot be determined due to the interference by dissociative ionization. The distribution has the peak located at 32 kcal/mol, and the maximum translational energy also

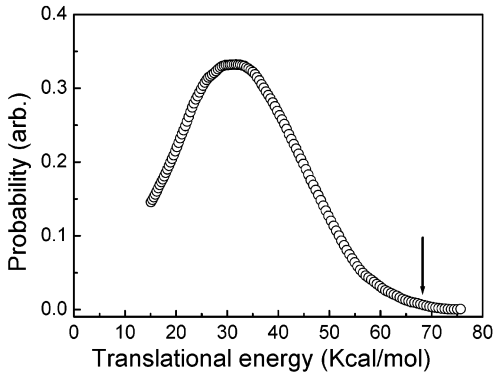

Figure 9. Photofragment translational energy distribution of the reaction $C_6D_5F + h\nu_{193nm} \rightarrow C_6D_4 + DF$. The arrow indicates the maximum available energy.

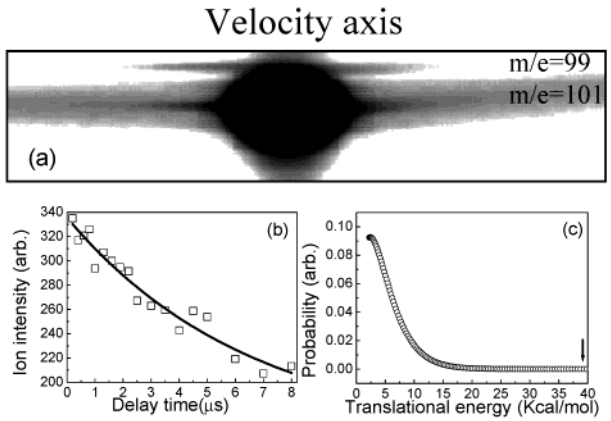

Figure 10. (a) Image and (b) image intensity decay of $m/e = 99$ ($C_6D_4F^+$) as a function of delay time. (c) Photofragment translational energy distribution of $C_6D_5F + h\nu_{193nm} \rightarrow C_6D_4F + D$. The arrow indicates the maximum available energy.

reaches the maximum available energy of the reaction $C_6D_5F \rightarrow C_6D_4 + DF$.

The image of $m/e = 99$ and 101 is shown in Figure 10a, corresponding to the fragment ion $C_6D_4F^+$ and parent ion, respectively. The image of $C_6D_4F^+$ is line shaped, indicating the existence of the D atom elimination channel. The change of $m/e = 99$ ($C_6D_4F^+$) ion intensity as a function of delay time, illustrated in Figure 10b, correlates to a dissociation rate of $(1.8 \pm 0.6) \times 10^5$ s^{-1}. The photofragment translational energy distribution of this channel is shown in Figure 10c. The small kinetic energy released, the monotonic decrease of the probability with increasing translational energy, and the slow dissociation rate are the typical characteristics of dissociation from a molecule undergoing internal conversion to the ground electronic state with no exit barrier.

V. Discussion

The photophysics and photochemistry processes of benzene have been studied extensively. It is thus interesting to compare the photodissociation of fluorobenzene to that of benzene. Benzene in the S_2 state produced by 200 nm excitation was found to undergo fast internal conversion to the S_0 and S_1 states with a lifetime of ~40 fs, and the decay of the highly vibrationally excited S_1 state produced from this internal conversion occurred within 5−10 ps.[45] Recently, the dissociation rate of benzene after 193 nm excitation under collision-free conditions was measured.[46] Dissociation rates as slow as 10^5 and 5×10^4 s^{-1}, corresponding to C_6H_6 and C_6D_6, respectively, were observed. The fast relaxation from the S_2 and S_1 states to S_0 and the slow dissociation rate suggest the dissociation occurs from the vibrationally excited ground electronic state after internal conversion. The ground-state potential energy surface of benzene for various dissociation channels has been calculated by ab initio methods,[1] as shown in Figure 11. The H elimination occurs without an intrinsic barrier. The other dissociation channel is the elimination of the hydrogen molecule leading to *o*-C_6H_4. This channel is less endothermic than the H atom elimination but has a high barrier. The calculation also shows that the transition state for the four-center 1,2-H_2 elimination from benzene converges to the transition state for the 1,1-H_2 elimination and connects the products, *o*-C_6H_4 and H_2. Thus, the H_2 elimination is preceded by the 1,2-H shift and then the three-center elimination. Although both H atom and H_2 molecular elimination are energetically possible, only H atom elimination was observed experimentally in photodissociation of benzene at 193 nm.[2] Dissociation occurring in the triplet state or from a different isomer has not been reported.

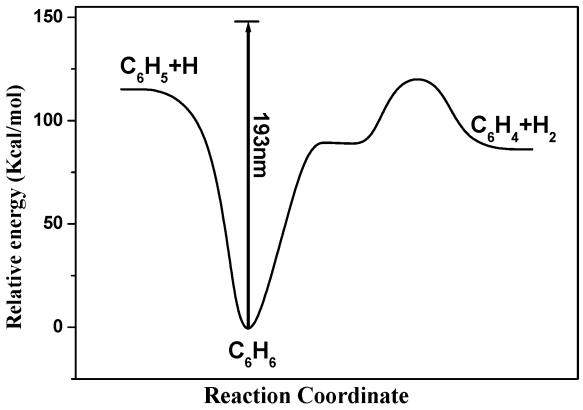

Figure 11. Energy diagram for isomerization and dissociation reactions of benzene from ref 1.

Our experimental results demonstrate that the replacement of one H atom by an F atom in benzene changes the dissociation properties significantly. UV absorption of 193 nm corresponds to the photoexcitation of fluorobenzene to the S_3 state. Dissociation occurs mainly through HF elimination, and only small amounts of molecules dissociate through H atom elimination. As a result, the experimental data can be described using the following reactions.

$$C_6H_5F + h\nu_{193nm} \rightarrow C_6H_5F^*(S_3) \quad \text{(excitation)} \tag{1}$$

$$C_6H_5F^* \rightarrow C_6H_5F^{\ddagger}(S_0) \quad \text{(internal conversion to } S_0\text{)} \tag{2}$$

$$C_6H_5F^{\ddagger} \rightarrow C_6H_4 + HF \quad \text{(dissociation from } S_0\text{)} \tag{3}$$

$$C_6H_5F^{\ddagger} \rightarrow C_6H_4F + H \quad \text{(dissociation from } S_0\text{)} \tag{4}$$

The dissociation products from reactions 3−4 were ionized by VUV laser and detected by an ion image detector. They can be represented by the following reaction:

(45) Radloff, W.; Freudenberg, Th.; Ritze, H. H.; Stert, V.; Noack, F.; Hertel, I. V. *Chem. Phys. Lett.* **1996**, *261*, 301−306.
(46) Tsai, S. T.; Lin, C. K.; Lee, Y. T.; Ni, C. K. *J. Chem. Phys.* **2000**, *113*, 67−70.

$$P + h\nu_{VUV} \rightarrow P^+ \ (P = C_6H_4, C_6H_4F) \qquad (5)$$

However, at a very short delay time, some of the excited fluorobenzene molecules that have not dissociated into fragments could absorb the VUV photon and result in dissociative ionization.

$$C_6H_5F^{\ddagger} + h\nu_{VUV} \rightarrow C_6H_4F^+ + H \qquad (6)$$

$$C_6H_5F^{\ddagger} + h\nu_{VUV} \rightarrow C_4H_3F^+ + C_2H_2 \qquad (7)$$

$$C_6H_5F^{\ddagger} + h\nu_{VUV} \rightarrow C_6H_4^+ + HF \qquad (8)$$

Similar reactions can be used to describe the photodissociation of C_6D_5F. The ion from the dissociative ionization channels (6−8) produces the background at a short delay time. The nonzero intensity of $m/e = 73$ and 76 at $t = 0$ and the intensity decay of $m/e = 95$ and 99 at a short delay time, as well as the disklike images, are all due to this background. However, at a long delay time, most of the excited fluorobenzene dissociates into fragments, and this background decays to zero. The decays we observed are all due the dissociation through reactions 3 and 4.

The fluorobenzene potential energy curves for various dissociation channels obtained by density functional B3LYP/6-31+G* calculations are shown in Figure 12. In addition to the F atom elimination through the C−F bond cleavage which is illustrated by a high dissociation threshold, the dissociation channels of the H atom elimination and HF elimination through the three-center reaction mechanism are very similar to those of H atom and H_2 molecule elimination channels in benzene. The H atom elimination can occur from three positions of the aromatic ring, and results in slightly different energies, as shown in Figure 12. The three-center HF elimination starts from the 1,2-H shift through the transition state TS2 and then HF elimination through transition state TS3. However, in contrast to the H_2 four-center elimination in benzene, the transition state of the HF four-center elimination in fluorobenzene does *not* converge to that of the three-center elimination and it has a very low barrier. It is this channel that makes the photodissociation of fluorobenzene very different from that of benzene. The HF bond distance in the transition state TS1 (1.09 Å) is very close to the product's HF bond distance (0.917 Å), compared to the long HF bond distance (1.67 Å) in the transition state TS2. The structures of both transition states TS1 and TS2 are shown in Figure 13. As a result, most of the fluorobenzene dissociate through HF four-center elimination due to the low barrier height, and the kinetic energy release is large because of the late barrier characteristics of the transition state TS1.

The dissociations of fluorobenzene in the ground electronic state are unimolecular reactions and they can be characterized with RRKM theory. We used the potential energy surface obtained from the density functional calculation and performed the RRKM calculation for various reaction rates. For the three-center elimination, the results of the RRKM calculation show that 1,2-H shift through TS2 has a rate of $9.6 \times 10^5\ s^{-1}$ and the reverse reaction has a rate of $6.5 \times 10^{12}\ s^{-1}$. The subsequent dissociation through TS3 to form the C_6H_4·HF complex is $1.5 \times 10^{10}\ s^{-1}$, and the reverse reaction is $1.1 \times 10^6\ s^{-1}$. The dissociation from the complex is very fast; our RRKM calculation indicates that it is faster than $10^{12}\ s^{-1}$. For the four-center elimination, the HF elimination through TS1 to form the C_6H_4·HF complex has a rate of $1.1 \times 10^6\ s^{-1}$, and the reverse reaction has a rate of $5.7 \times 10^8\ s^{-1}$.

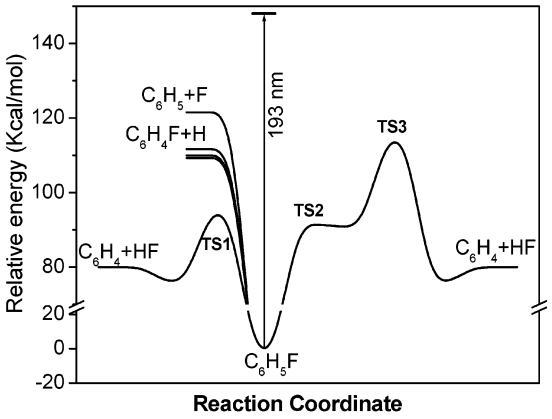

Figure 12. Energy diagram for isomerization and dissociation reactions of fluorobenzene. The energies are computed at CCSD/6-311+G* at the geometry optimized by B3LYP/6-31+G*.

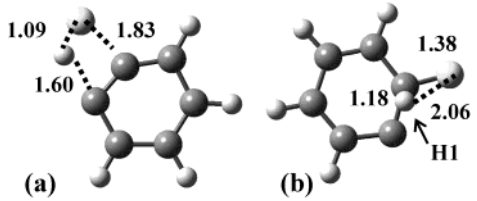

Figure 13. (a) Structure of transition state TS1. (b) Structure of transition state TS3. All the atoms are located very close to a plane, except one H atom in TS3 with the label H1.

Since the lifetime of the C_6H_4·HF complex is very short, we can neglect its reverse reactions via TS3 and TS1 and assume that once the complex is formed, it dissociates into $C_6H_4 + HF$ products, which fly apart and do not react again under collision-free conditions. Then, the rate constant for the product formation from the four-center elimination is $1.1 \times 10^6\ s^{-1}$. For the three-center elimination, we can use the steady-state approximation (for the intermediate formed after the 1,2-H shift) and calculate the total rate constant for the $C_6H_5F \rightarrow$ TS2 $\rightarrow$ intermediate $\rightarrow$ TS3 $\rightarrow C_6H_4 + HF$ process. This calculation gives $2.2 \times 10^3\ s^{-1}$; that is, the three-center elimination is much slower than the four-center elimination.

Next, we carried out similar calculations for C_6D_5F. Due to the difference in zero-point energies, the reaction barriers in this case are slightly higher, which results in somewhat lower rate constants. For instance, the rate for the four-center DF elimination via TS1 is $2.7 \times 10^5\ s^{-1}$, while the overall rate for the three-center elimination via TS2 and TS3 (assuming steady-state conditions) is $3.65 \times 10^2\ s^{-1}$. As for HF, the four-center DF elimination is much faster than the three-center elimination. Assuming that the four-center elimination is the dominant reaction process, we calculated the lifetime of C_6F_5F as $0.9\mu s$ and that of C_6D_5F as $3.7\mu s$. These values are in good agreement with the experimental lifetimes.

In conclusion, we demonstrate that (1) the dissociation rates of C_6F_5F and C_6D_5F can be obtained from the product growth and intensity decay of disklike images at various delay times, (2) the kinetic energy released in the HF and C_6H_4 fragments reaches the maximum available energy, indicating the dissocia-

tion occurs in the ground electronic state, (3) high intensity of the C_6H_4 fragment suggests that HF elimination is the major dissociation channel, and (4) calculations from ab initio results show that the four-center HF elimination is the major reaction channel. Compared to the previous studies of aromatic molecules, including benzene, alkyl-substituted and halogen atom-substituted benzenes, fluorobenzene is the only aromatic molecule which produces two close shell fragments in this photon energy region.

Acknowledgment. The work was partly supported by the National Science Council of the Republic of China, under Contract NSC 91-2113-M-001-023.

JA030185K